Composition, Structure, and Electric Field Variations in Photodeposition

R. J. Wilson and F. A. Houle
IBM Research Laboratory, San Jose, California 95193
(Received 25 June 1985)

Copper-carbon films formed by photodeposition from a vapor-phase copper-organic compound by use of a cw ultraviolet laser beam exhibit periodic ripple structures associated with surface waves. Microscopic analysis of these films shows that composition and order also vary periodically and change abruptly on dimensional scales small compared to optical wavelengths. A simple model including strongly varying fields appropriate to the film corrugation is proposed to explain these unusual features.

PACS numbers: 68.55.+b, 71.45.Gm, 78.65.Ez

The formation of periodic structures, or ripples, on surfaces exposed to laser radiation has been observed for optically damaged surfaces[1-5] and photochemically deposited films.[6,7] Although it is generally agreed that ripple formation involves scattering of the incident beam into surface waves, the details of how the surface electromagnetic waves actually effect changes in the photodeposition process have only been explored for the $(CH_3)_2Cd$ system.[6-8] In this Letter we present data showing that the processes involved in ripple formation during metal photodeposition are more general and can exhibit far richer detail than previously suggested. Our films show novel properties, including periodicity in composition and crystallinity, in addition to the topographic variations described by others.

The photodeposited films studies were grown by photolysis of (Cu II)(1,1,1,5,5,5,-hexafluoropentanedione)$_2$(ethanol).[9] Solid samples of this compound were introduced into a stainless-steel vacuum cell which was subsequently evacuated to the vapor pressure ($\simeq 10$ μm) of the solid. A cw beam at 257 nm, obtained from a doubled argon-ion laser, was focused to a 10-μm-diam spot at nominal power densities of $(1-2)\times 10^4$ W/cm^2. Under these conditions photodeposition is primarily due to photolysis of molecules at or near the substrate surface. Films of varying thickness have been deposited on native oxide-covered silicon wafers and carbon-coated cleaved mica by use of growth times ranging from 5 to 30 min. Films grown with use of a 514-nm light at intensities where substrate heating is important show no ripple structure and are composed of high-purity copper crystallites.[10] We have used scanning electron microscopy (SEM), scanning Auger microscopy (SAM), and transmission electron microscopy (TEM) in order to characterize the composition and structure of the uv-deposited films and to understand the origin of ripple structures and their relationship to local surface photochemistry.

Figure 1(a) is an SEM micrograph of the edge of a thick spot (0.5 μm) on Si which displays many of the topographic features usually observed.[7] The fine vertical ripples are closely spaced ($\simeq 1500$ Å) in area (1), farther apart in area (3), and oriented at right angles to the laser polarization. More widely spaced ripples, area (2), running parallel to the laser polarization, and fairly large ellipsoidal structures are also evident. Figure 1(b) shows integral Auger spectra taken after sputter cleaning which indicate that the film surface is nearly 50% carbon in region I and 90% carbon in region II. Negligible composition changes were detected even for sputter depths in excess of 300 Å.

To analyze local concentrations, peak and background count rates for Cu and C were recorded while

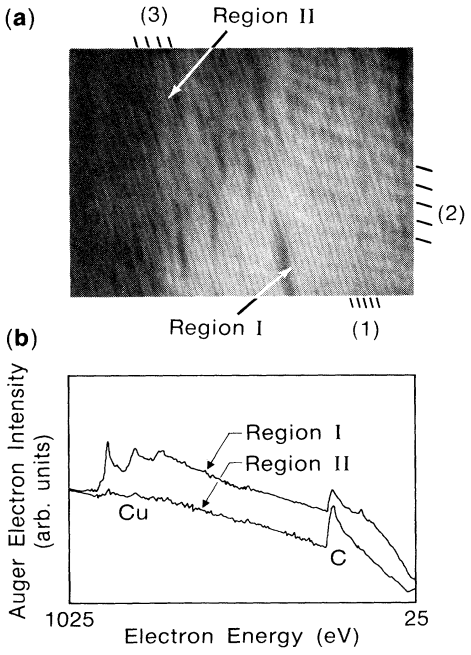

FIG. 1. (a) SEM micrograph of a portion of a photodeposited spot showing finely spaced ripples, (1) and (3), and more widely spaced transverse (2500 Å) ripples, (2). (b) Low-spatial-resolution integral Auger spectra of regions I and II. An approximate calibration, obtained by the neglect of escape depth and backscattering variations between the two regions, gives carbon concentrations of about 0.9 and 0.4 for the two regions. Small amounts of F and Cl, as seen here, are detected occasionally.

the beam was scanned across topographic features. Results for several sputter-cleaned samples are shown in Fig. 2 to demonstrate that strong composition variations are observed, even on the 1000-Å scale. It is difficult to quantify the elemental concentration because peak and background signals both show strong oscillations of topographic origin; hence the ratio of Auger signals is plotted. The fine-fringe composition modulation, trace *c*, represents a lower limit, as spatial resolution (≈ 500 Å) and sample drift both wash out the variation. The copper-rich regions are found to coincide with the ripple peaks observed in SEM images.

In order to obtain higher spatial resolution and structural information, thin spots (≈ 1000 Å) were deposited at low intensity for TEM examination. Bright-field micrographs of a carbon-supported spot are shown in Fig. 3. Near the edge a sinusoidal ripple structure of short wavelength is observed with ~ 100-Å clusters of ~ 20-Å grains. The center of the spot is distinguished by the appearance of large (≈ 100-Å) grains arranged in neat rows along the minima of a more gentle modulation. Selected-area diffraction patterns taken near the edge and dark-field images of the grain rows demonstrate that the granular features are not primarily metallic and are more ordered than the surrounding matrix. It is also evident that the spatial coherence of the ripples is poor, since ripples frequently divide and shift phase over a few grating wavelengths.

These data conclusively demonstrate that films obtained by photodeposition from (Cu II)(1,1,1,5,5,5-hexafluoropentanedione)$_2$(ethanol) are nearly amorphous copper-carbon composites which show periodicity in composition, topography, and crystallinity. Studies of the average composition of copper-carbon films deposted over a range of incident light intensities have shown that a major source of carbon is decomposition of the ligands and incorporation of the products into the growing film.[9] The percentage of carbon increases with decreasing light intensity in the power-density regime used for these experiments. The microscopic and macroscopic composition variations observed indicate that copper-rich regions coincide with electromagnetic-field maxima at the surface.

Observations of ripple formation in metal photodeposition have previously been ascribed to surface-plasma wave scattering,[6] which occurs when a plane wave at normal incidence strikes a greatly corrugated surface, resulting in a surface electric-field component

$$E_x^{\mathrm{TM}} = E_x^{\mathrm{inc}} t\left[1 + \left(k_1 + \frac{\gamma_1\gamma_0(1-\epsilon)}{(\gamma_0\epsilon+\gamma_1)}\right) h\cos(kx)\right]. \quad (1)$$

Here k_0 is the incident wave vector, $\mathbf{k} = k\hat{\mathbf{x}}$ is the grating wave vector, $\gamma_0 = (k^2 - k_0^2)^{1/2}$, $\gamma_1 = (k^2 - \epsilon k_0^2)^{1/2}$, and $k_1 = \sqrt{-\epsilon}k_0$, with $\mathrm{Re}\gamma_0, \gamma_1 > 0$ and $\mathrm{Re}\epsilon < 0$; $t = 2k_0/(k_0 + ik_1)$ is the normal-incidence Fresnel transmission coefficient and E^{inc} is the incident field. If the film-growth rate is taken to be proportional to $|E|^2$ and small terms are dropped, then the exponential ripple growth can be obtained in terms of the film-thickness growth rate, dT/dt, from $dh/dt = (dT/dt)\,\mathrm{Re}(m)h$. The gain factor m is the coefficient of $h\cos(kx)$ within the brackets in (1) and has a pole when $k = k_0[\epsilon/(\epsilon+1)]^{1/2}$, which can lead to resonantly enhanced ripple growth. This model is

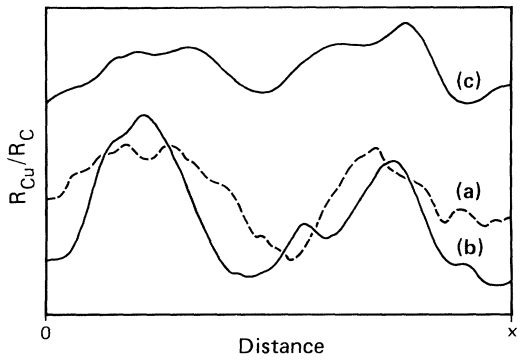

FIG. 2. Auger line-scan data taken for scans over topographic features of various dimensions. Trace *a* was obtained for a gross feature with $x = 3$ μm; trace *b* was observed for a pair of adjacent anomalously wide ripples similar to structures seen in Fig. 3 for $x = 0.7$ μm. Trace *c* resulted from a scan over finely spaced ripples with $x = 0.3$ μm. Statistical errors are negligible compared to variations between different samples or areas within the same spot.

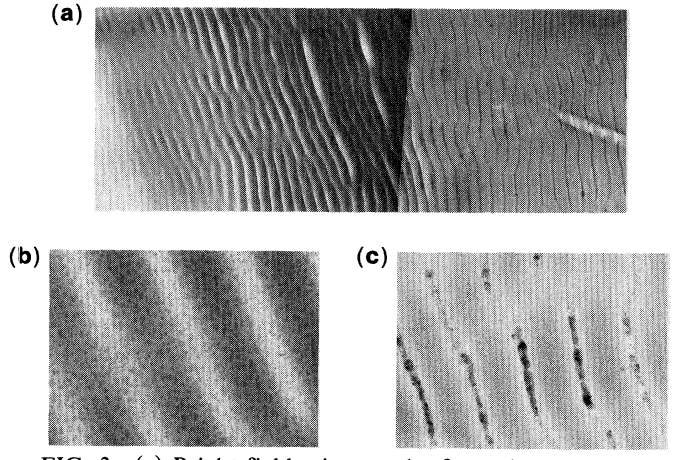

FIG. 3. (a) Bright-field micrograph of a region extending from the deposit edge at left into the central-spot region at the right. (b) A higher-magnification view of the weak corrugation and clustered grain structure observed near the spot edge (ripple spacing ≈ 1100 Å); (c) well-developed grain rows in the minima of a corrugated matrix of fine grains as observed in the spot center (ripple spacing ≈ 1800 Å).

helpful for the understanding of the exponential gain and observed polarization but does not offer a clear picture of initial growth or of the range of materials for which ripple formation is expected, especially since ϵ cannot be obtained directly from the grating wavelength for lossy materials. It appears that the existence of grating wave vectors larger than k_0 requires $\mathrm{Re}(\epsilon) < -1$, but the exponential growth calculated from (1) evidently persists even for very heavy damping. It is noteworthy that a value of ϵ in this range is expected for both glassy and graphitic carbon at uv frequencies but as a consequence of strong π electron absorption rather than a metallic response.[12] Thus dielectric constants with negative real parts and substantial imaginary parts corresponding to strong uv absorption are not unreasonable for our films, but large resonant enhancements and collective surface excitations are highly unlikely. Our observations of a correlation between increasing grating wave vector and increasing average copper concentration (Fig. 1) suggest that ϵ should be considered an unknown and locally variable parameter.

In the case of inhomogeneous absorbing media, where only partially coherent ripple patterns of varying wavelength are observed, the intuitive value of Fourier techniques such as (1) diminishes because many amplitudes and phases must be considered. Since the phenomena observed here are qualitatively similar to predictions for undamped homogeneous media, it appears likely that even in complex systems ripple evolution can be traced back to the microscopic properties of the deposited films and the nature of radiation from individual dipole scatterers. This approach is particularly interesting from the point of view of initial growth where two-dimensional radiation from small nucleation sites must transform itself into one-dimensional radiation characteristic of ripple patterns. To develop such a microscopic description, the nascent film is taken to be a fine-grained metal-carbon matrix which has fluctuations in surface topography, grain size, and metal content. The electric fields generated by individual grains or bumps must be considered carefully, since it is well known that such structures can produce enhanced fields through either Mie resonance effects or shape-dependent lightning-rod enhancements.[13,14] Resonance effects on the electric field just outside an individual grain can produce asymmetric grain growth, which has been observed previously for the $(CH_3)_2Cd$ system.[8] The lightning-rod effect could result in large electric fields, particularly at sharp edges in the grain rows. The only possible manifestation of either effect is the crystalline grain which develops only in thick corrugated regions. We therefore ignore these effects and discuss a simple continuous-medium model for initial growth.

To understand the development of linear ripples, we consider radiation from a horizontal dipole induced by the laser at a planar interface by using the Hertz potential, Π, from which the field $\mathbf{E} = k_0^2 \Pi + \nabla(\nabla \cdot \Pi)$ can be derived.[15,16] The result for Π at a flat surface for a point dipole at the origin is

$$\frac{\Pi}{p} = \hat{\mathbf{x}} \int_{-\infty}^{\infty} \frac{H_0^1(k\rho)\, k\, dk}{\gamma_0 + \gamma_1} + \hat{\mathbf{z}} \frac{1}{k_0^2} \frac{\partial}{\partial x} \int_{-\infty}^{\infty} \frac{(\gamma_0 - \gamma_1)}{\epsilon\gamma_0 + \gamma_1} H_0^1(k\rho)\, k\, dk, \tag{2}$$

where p is the dipole moment, $\rho = (x^2 + y^2)^{1/2}$, and H_0^1 is a cylindrical Hankel function. The second term, Π_z, has a pole at $\epsilon_1\gamma_0 + \gamma_1 = 0$ which contributes a term

$$\Pi_z^{\mathrm{sw}} = [2\pi i \epsilon p \gamma_0^2 / k_0^2 (\epsilon - 1)] \partial H_0^1(k\rho)/\partial x.$$

In the asymptotic limit of large $k\rho$ we find

$$E_x^{\mathrm{sw}} = \cos^2\phi [\sqrt{8}\pi p \gamma_0^3 \epsilon^2 / (1 - \epsilon^2)] (k\rho)^{-1/2} e^{-i(k\rho + \pi/4)}.$$

This radiation field falls off with a $\rho^{-1/2}$ dependence characteristic of a two-dimensional surface wave and will give rise to a cylindrical ripple pattern along the primary grating direction since $\cos\phi = x/\rho$.

If each point of the resulting fan-shaped ripple pattern is treated as a source of dipole radiation, then the field at the origin can be further increased, leading to positive feedback.[17] An approximate calculation of the field at the point ρ', θ near the origin involves $\int_0^{2\pi} \cos^4\phi e^{ik\rho' \cos(\theta - \phi)} d\phi$ and shows that the field extends farther along the y axis than the x axis as a consequence of the directed nature of the radiation field. There is thus an intrinsic tendency for an initial point source to elongate along the ripple direction and to assume a one-dimensional character as a consequence of the radiation from sources produced by the original field. As the surface roughens, one must consider the generalization of (2) to include vertical displacements of sources and deposition sites. In this case the cancellation of the usual dipole potential is broken, giving an extra term[15] $\Pi_x = e^{ik_0 R_+}/R_+ - e^{ik_0 R_-}/R_-$, where $R_\pm = [r^2 + (z - h)^2]^{1/2}$, with z and h the height of the surface at ρ, ϕ and at the dipole, respectively. This term clearly leads to radiation at wave vector k_0 which peaks in the y-x plane and should generate ripples running parallel to the incident polarization. This is consistent with the structures

shown in Fig. 1.

None of the models presented provides an explanation for the formation of the grain row structures in the ripple minima. Since crystallites only appear near the spot edge or in the grain rows, it appears that the unique development of large grains at the ripple minima in thick regions of the film is associated with strongly reduced light intensities. Several factors may contribute to their formation. The local surface composition may also play a role by influencing adsorption and reaction steps, leading to chemical feedback. The appearance of a crystalline phase could trigger local field effects which depend critically upon microstructure. Such effects have been proposed to account for narrow ripple structures observed in optical-damage studies.[18] These fields will in turn influence the photolytic process, possibly resulting in instabilities and transient effects. The growth of large crystallites at ripple minima, and not near the spot edge, might then be favored by local field structures which involve the spatially oscillating fields generated by the ripples and the narrow grain-row structures. To understand the development of grain rows more fully, it will be necessary to quantify possible effects of local film structure and composition on local fields, adsorption, and photolysis.

Our results demonstrate that composition, structure, and dielectric constant inhomogeneities together with details of surface photolysis and grain-growth mechanisms must all be known before reasonable predictions for other photochemical systems can be made. Our observations on primarily carbon films show that ripple generation does not depend on nor imply metallic properties. Rather, the development of surface ripples may be associated with irradiation near strong absorption bands of the parent and product compounds together with dipolar scattering. Furthermore, if the photolysis and film-growth mechanism involve several competitive thermal and photochemical reaction pathways whose branching ratio depends on the local light intensity, then variations in fields at the surface will lead to variations in film composition and morphology. The complexity of phenomena observed suggests that deliberate spatial or temporal variations of incident intensity can be useful for the obtaining of nucleation sites or distinct phases within photodeposited films. Similar effects may be obtained for photodeposition of a wide variety of materials, particularly multicomponent systems containing carbon.

We are most grateful to V. Hanchett and R. Geiss for the TEM analysis. We would also like to thank H. Morawitz for helpful discussions.

[1]J. E. Sipe, J. F. Young, J. S. Preston, and H. M. van Driel, Phys. Rev. B **27**, 1411 (1983).

[2]J. F. Young, J. S. Preston, H. M. van Driel, and J. E. Sipe, Phys. Rev. B **27**, 1155 (1983).

[3]Z. Guosheng, P. M. Fauchet, and A. E. Siegman, Phys. Rev. B **26**, 5366 (1982).

[4]F. Keilmann and Y. H. Bai, Appl. Phys. A **29**, 9 (1982).

[5]D. J. Ehrlich, S. R. J. Brueck, and J. Y. Tsao, Appl. Phys. Lett. **41**, 630 (1982).

[6]S. R. J. Brueck and D. J. Ehrlich, Phys. Rev. Lett. **48**, 1678 (1982).

[7]R. M. Osgood, Jr., and D. J. Ehrlich, Opt. Lett. **7**, 385 (1982).

[8]C. J. Chen and R. M. Osgood, Phys. Rev. Lett. **50**, 1705 (1983).

[9]C. R. Jones, F. A. Houle, C. A. Kovac, and T. H. Baum, Appl. Phys. Lett. **46**, 97 (1985).

[10]F. A. Houle, C. R. Jones, T. H. Baum, C. Pico, and C. A. Kovac, Appl. Phys. Lett. **46**, 204 (1985).

[11]V. Celli, A. Marvin, and F. Toigo, Phys. Rev. B **11**, 1779 (1975).

[12]E. A. Taft and H. R. Philipp, Phys. Rev. **138**, A197 (1965).

[13]A. Nitzan and L. E. Brus, J. Chem. Phys. **75**, 2205 (1981).

[14]R. Ruppin, Solid State Commun. **39**, 903 (1981).

[15]A. Sommerfeld, *Partial Differential Equations in Physics* (Academic, New York, 1949).

[16]J. A. Stratton, *Electromagnetic Theory* (McGraw-Hill, New York, 1941).

[17]P. A. Temple and M. J. Soileau, IEEE J. Quantum Electron. **17**, 2067 (1981).

[18]Jeff F. Young, J. E. Sipe, and H. M. van Driel, Phys. Rev. B **30**, 2001 (1984).

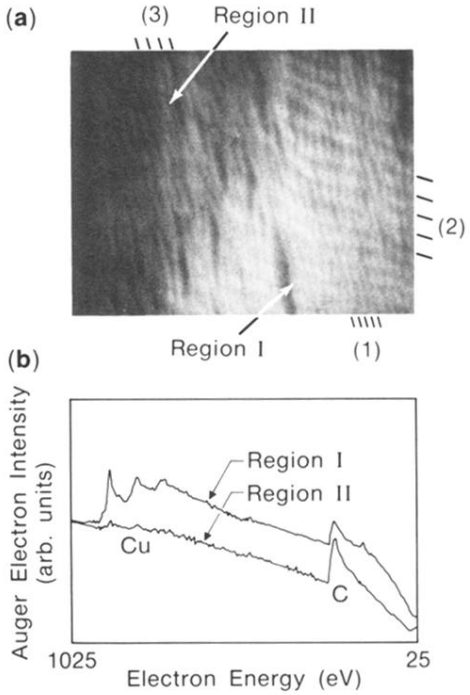

FIG. 1. (a) SEM micrograph of a portion of a photodeposited spot showing finely spaced ripples, (1) and (3), and more widely spaced transverse (2500 Å) ripples, (2). (b) Low-spatial-resolution integral Auger spectra of regions I and II. An approximate calibration, obtained by the neglect of escape depth and backscattering variations between the two regions, gives carbon concentrations of about 0.9 and 0.4 for the two regions. Small amounts of F and Cl, as seen here, are detected occasionally.

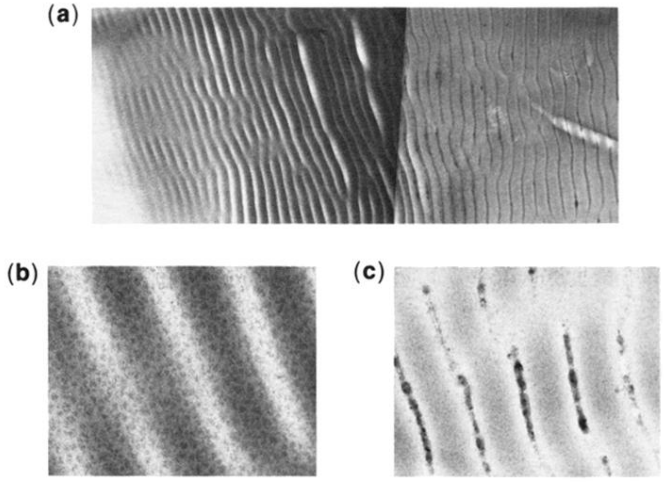

FIG. 3. (a) Bright-field micrograph of a region extending from the deposit edge at left into the central-spot region at the right. (b) A higher-magnification view of the weak corrugation and clustered grain structure observed near the spot edge (ripple spacing ≈ 1100 Å); (c) well-developed grain rows in the minima of a corrugated matrix of fine grains as observed in the spot center (ripple spacing ≈ 1800 Å).